DISCUSSION ON ONE ALGORITHM FOR MAPPING THE RADIATION DISTRIBUTION ON CONTAMINATED GROUND

Ruirui Liu,*† Kathryn Higley,† and Xinzhi Liu*

Abstract—**Recently, due to progressions in radiation detection systems, the capability to monitor radiation on the ground by employing detection systems high above the ground has been developed. Therefore, how to map radiation distributions on the ground based upon measured data in air is an important question. One kind of reconstructing algorithm for solving this problem is introduced in this paper. This algorithm reconstructs the radiological contamination distribution through solving the detection response factors equation set (DRFES). The study shows that the reconstructing algorithm performs well when the detection height is lower than 50 m. Through this algorithm, the ability to reconstruct the scope of contamination magnitude on the ground by using the measurement data obtained in the air has been established. The algorithm discussed in the paper has the potential to be used in emergency monitoring and nuclear decontamination.**
Health Phys. 109(1):25–34; 2015

Key words: accidents, nuclear; emergency planning; gamma radiation; modeling, environmental

INTRODUCTION

ONE IMPORTANT task for responding to radiological and nuclear accidents is emergency monitoring; effective emergency monitoring can help first responders handle the situation more properly and safely. Obtaining the radiation distribution on the contaminated ground can help the first responders to set up different response zones. With this, it is clear why proper measurements and analysis of the radiation distribution on the ground play a key role in emergency monitoring. There are various types of scenarios that have a need for emergency monitoring; for example, a terrorist attack by detonation of radiological dispersal devices (RDD), a radiological accident (IAEA 1988), or a nuclear accident in a nuclear power plant (Sanada et al. 2014). Furthermore, apart from the initial measurements, how to map the radiation distribution on the contaminated region accurately during the decontamination mission stage deserves research attention.

Recently, a lot of research has been completed for the development of monitoring systems, such as the development of monitoring systems based on unmanned aerial vehicles (Okuyama et al. 2005; Pollanen et al. 2009; Bogatov et al. 2013) and the development of vehicular ground-based monitoring systems (Long et al. 2004). However, little attention has been paid to the development of accurate and powerful radiation mapping algorithms based upon the measurement data acquired by these monitoring systems.

During monitoring, the vehicle-mounted and plane-mounted monitoring systems were used to measure the radiation in the air. However, sometimes the radiation distribution on the ground bears more valuable function for emergency zoning and post decontamination. Therefore, how to reconstruct the radiation information (i.e., surface activity) based upon the radiation information in the air deserves research attention. In this work, an algorithm was developed to reconstruct the radiation surface activity from the radiation information in air. The overall development for this specific algorithm is below.

DEVELOPMENT OF THE ALGORITHM

Assumptions and parameter optimization

In order to develop this algorithm, some reasonable assumptions were made. They are as follows:

- the assumption that the radiation is distributed in one finite plane surface;
- the neglect of radiation measurement contribution from the suspended airborne radioactive particles; and
- the fact that each measurement was taken with the detector maintained at a fixed location on ground.

The reason for neglecting the suspended airborne radioactive particles is that those particles will drop down to

*Department of Radiation Safety, China Institute of Atomic Energy, Beijing, 102413, China; †Department of Nuclear Engineering and Radiation Health Physics, Oregon State University, 100 Radiation Center, Corvallis, OR 97331.

The authors declare no conflicts of interest.

For correspondence contact: Ruirui Liu, Oregon State University, Corvallis, OR 97331, or email at **liuru@onid.oregonstate.edu**.

(*Manuscript accepted* 2 *February* 2015)
0017-9078/15/0

DOI: 10.1097/HP.0000000000000289

the ground after a reasonably long time due to wet or dry deposition, and also the natural background airborne radioactivity due to cosmic rays and radon decay is quite small compared to the radioactivity of interest in the survey. The method proposed in this work is basically for a helicopter-mounted detection system, since the helicopter can stop in one specific location, just measure the radioactivity in that location, and move to the next location when current measurement is finished.

There are numerous monitoring schemes for use; however, the easiest one is moving the detector following predefined square grids as shown in Fig. 1. As displayed in Fig. 1, *i* and *j* are the indexes used to describe grid *G*, so *G*(*i, j*) is a specific point on the grid, and *W* is the width of grid distance. In this monitoring scheme, the detector will measure the radiation in the air at the grid points following the defined monitoring route. For instance, the detector will make a measurement at location *O* and, once completed, will move to the next measurement point in the grid where the next radiation measurement will be obtained. During the field monitoring, the vehicle will move at a specific speed, allowing the detector to actually measure just at the grid point if the measurement time cycle has been set up appropriately.

It is important to note that the uniform rectangular grid proposed in this method is idealized, because positioning the measurement platform is not easily controlled in a real situation. However, the applicability of this method will not deteriorate, since the measured data could be interpolated to create a rectangular grid mathematically, although the flying platform did not follow the rectangular grid lines. These post-measurement interpolated rectangular grid data could also be used to reconstruct the radiation distribution based on this method.

During monitoring, the detector is working at a certain height above ground; suppose the height is *h* (as shown in Fig. 2) and the grid width is *W*. The grid width determines the reconstructed resolution for surface activity, which also in turn determines the monitoring cost, since more grids means more monitoring time and radiation exposure risk for the monitoring system operators. Therefore, it is worthwhile to optimize the grid width based upon the detection height and reconstruction resolution. As shown in Fig. 2, suppose the surface activity concentration is A_0/m^2; then the activity in an infinitesimal area ds is A_0ds. Since $ds = rdrd\varphi$, then the count rate measured from an activity emitted in area ds is

$$d\dot{N} = \frac{A_0 rdrd\varphi\Omega(r)\varepsilon}{4\pi} e^{-uR}, \quad (1)$$

where $\Omega(r)$ is a full detection solid angle for this infinitesimal area, R is the distance from the infinitesimal area to the detector, μ is the air attenuation factor, and ε is the intrinsic efficiency of the detector. Since the detector usually is high enough above the infinitesimal area, one can simplify that the detector is circular. According to the geometry shown in Fig. 2, the full detection solid angle is

$$\Omega(r) = 2\pi\left(1 - \frac{\sqrt{r^2+h^2}}{\sqrt{r^2+h^2+a^2}}\right), \quad (2)$$

where r is the lateral distance from detector, h is the detector height from ground, and a is the effective detector radius. With this, the count rate from this infinitesimal radioactive contaminated area is

$$d\dot{N} = \frac{A_0\varepsilon}{2} r\left(1 - \frac{\sqrt{r^2+h^2}}{\sqrt{r^2+h^2+a^2}}\right) e^{-u\sqrt{r^2+h^2}} d\varphi dr. \quad (3)$$

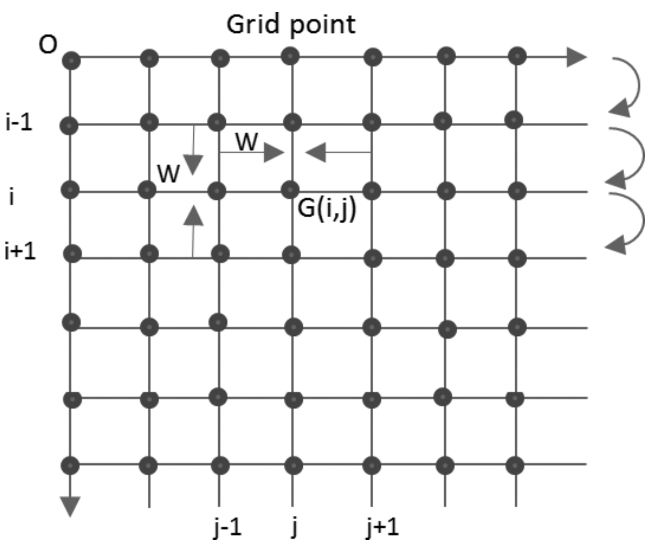

Fig. 1. The measuring grid distribution.

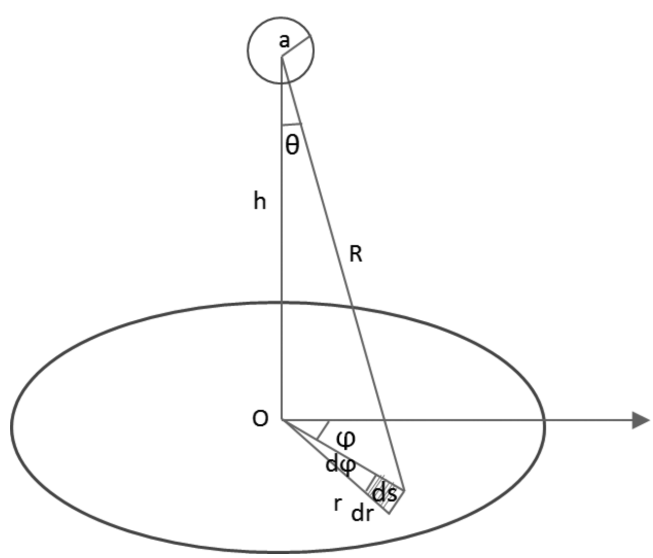

Fig. 2. Detection layout.

If the lateral distance is x, then the total count rate is an integration of eqn (3):

$$\dot{N}(x) = \pi A_0 \varepsilon \int_0^x r\left(1 - \frac{\sqrt{r^2+h^2}}{\sqrt{r^2+h^2+a^2}}\right) e^{-u\sqrt{h^2+r^2}} dr. \quad (4)$$

Also, it is noteworthy that the build-up factor was not considered in eqn (4) since the build-up effect on the count rate will be canceled out in eqn (5).

In order to determine the optimized grid width W, it is best to define a saturation distance L. This saturation distance L can be solved from eqn (5) coupled with eqn (4):

$$R(L) = \frac{\dot{N}(L)}{\dot{N}(\infty)} = 90\%. \quad (5)$$

Since the detector is symmetrical with the distance r, then the grid width should be determined by eqn (6):

$$W = 2L, \quad (6)$$

where $R(L)$ is the saturation ratio, $\dot{N}(L)$ is the count rate when the detection region radius is L, and $\dot{N}(\infty)$ is the count rate when the detection region radius is infinitely long. It is reasonable to consider that 90% is enough statistically to represent the measurement contribution from the infinite detected area, since the remaining 10% represents the contribution by the remaining area out to an infinite distance from the detector.

It is noteworthy to mention that in real field monitoring, the number (such as 90%) of the saturation ratio could be adjusted according to the measurement work assessment. The larger the saturation ratio, the larger the grid width will be. Less measurement work will be needed since there will be less monitoring track for a specific monitoring area. This is understandable from a mathematical perspective. On the other hand, the smaller the saturation ratio, the smaller the grid width. Then more measurement work will be needed since there will be more monitoring track for a specific monitoring area; however, the more accurate distribution data could be reconstructed numerically.

Here, taking an unmanned vehicle-mounted monitoring system as an example, the relationship between saturation ratio and lateral distance from the detector was analyzed and is shown in Fig. 3. In this example, one can assume that the surface contamination is ^{137}Cs and the effective radius of the detector is 5 cm. Fig. 3 displays that the saturation ratio distribution is different when the detector height from ground is different. The higher the detector is, the shorter the saturation distance is. During field monitoring, the monitoring crew can determine the detection grid width by analyzing the saturation distance. The detection grid width should not be set up to be wider than two times the saturation distance; otherwise, some of the contaminated area on the ground will not be detected. The grid width can be set up as narrow as two times the saturation distance; however, the finer grid means higher detection costs (i.e., detection time).

Development of detection response factors equation set (DRFES)

Note the following: grid $G(i, j)$ is the grid at ith row, jth column; $\dot{N}(i, j)$ is the count rate recorded at position (i,j) on the grid as read by the detector; and $A(i, j)$ is the activity in the ground at grid position (i,j). Through the analysis of experimental results, it was found that the count rate at each

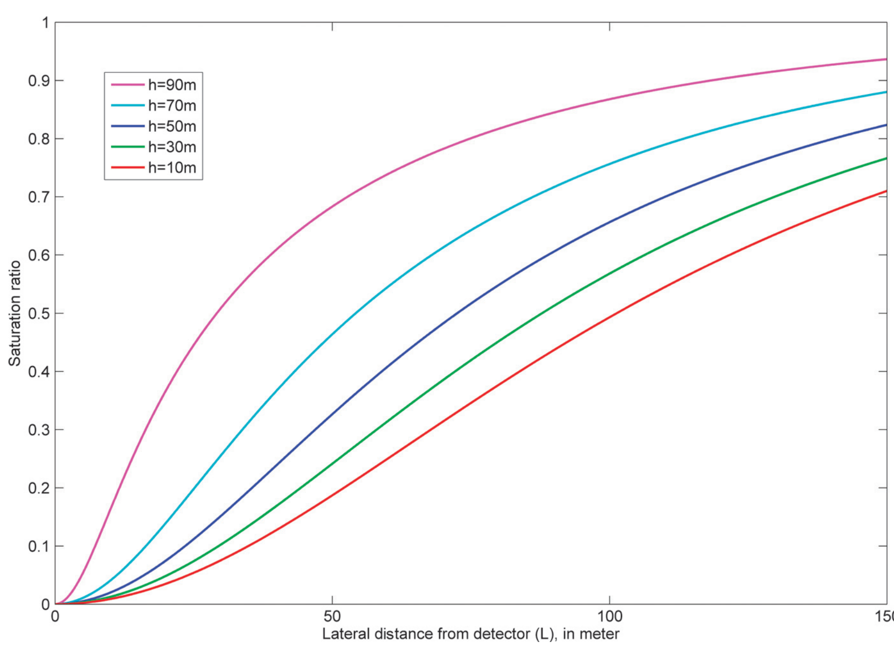

Fig. 3. Saturation ratio vs. lateral distance from detector (for ^{137}Cs contamination).

grid point is determined by the radiation activity at all individual grid points, which was mathematically illustrated in eqn (7). The authors denote $f_{i,j}^{I,J}$ as the response factor for grid position $G(i, j)$ to the detector when the detector is above the grid at $G(I, J)$. With this, it is known that the response factor presented is nothing but the total efficiency of the detector. For the count rate data in all grids, one can get following equation set:

$$\begin{cases} \dot{N}_{11} = f_{1,1}^{1,1}A_{11} + f_{1,2}^{1,1}A_{12} + \ldots + f_{n,n}^{1,1}A_{nn} \\ \dot{N}_{12} = f_{1,1}^{1,2}A_{11} + f_{1,2}^{1,2}A_{12} + \ldots + f_{n,n}^{1,2}A_{nn} \\ \ldots\ldots \\ \dot{N}_{ij} = f_{1,1}^{i,j}A_{11} + f_{1,2}^{i,j}A_{12} + \ldots + f_{n,n}^{i,j}A_{nn} \\ \ldots\ldots \\ \dot{N}_{nn} = f_{1,2}^{n,n}A_{11} + f_{1,2}^{n,n}A_{12} + \ldots + f_{n,n}^{n,n}A_{nn}. \end{cases} \tag{7}$$

If the above equation set is written in matrix form, it looks like this:

$$\dot{N} = F.A, \tag{8}$$

where

$$\dot{N} = \begin{bmatrix} \dot{N}_{11} \\ \dot{N}_{12} \\ \vdots \\ \dot{N}_{ij} \\ \vdots \\ \dot{N}_{nn} \end{bmatrix}_{nn\times 1}, \quad A = \begin{bmatrix} A_{11} \\ A_{12} \\ \vdots \\ A_{ij} \\ \vdots \\ A_{nn} \end{bmatrix}_{nn\times 1}, \quad F = \begin{bmatrix} f_{1,1}^{1,1} & f_{1,2}^{1,1} & \cdots & f_{i,j}^{1,1} & \cdots & f_{n,n}^{1,1} \\ f_{1,1}^{1,2} & f_{1,2}^{1,2} & \cdots & f_{i,j}^{1,2} & \cdots & f_{n,n}^{1,2} \\ \vdots & \vdots & & \vdots & & \vdots \\ f_{1,1}^{n,n} & f_{1,2}^{n,n} & \cdots & f_{i,j}^{n,n} & \cdots & f_{n,n}^{n,n} \end{bmatrix}_{nn\times nn}.$$

In equation (7), vector $\dot{N}$ could be obtained by measurements, while the response factor matrix, F, could be obtained by experimental measurements or analytical methods. Experimental measurements may get more accurate response factors for the detector; however, this specific methodology is more complicated and time consuming for emergency monitoring. Because of this increase in time consumption and overall complication, a simple solution that takes both accurate performance and time limitations will be provided in this paper.

According to the geometry of the grid, the distance between grid points $G(i, j)$ and $G(I, J)$ is $\sqrt{(i-I)^2+(j-J)^2}L$. When the detector is above grid point $G(i, j)$ [and since the grids maintain space translation symmetry, if any two grid points whose distance to grid point $G(i, j)$ are equal], then the response factors of these two grid points are equal. Mathematically, the relationship could be displayed as eqn (9):

$$f_{i,j}^{I,J} = f_{1,1}^{(1+|i-I|),(1+|j-J|)}, \tag{9}$$

where $f_{i,j}^{I,J}$ is the response factor for grid $G(I, J)$ when the detector is above grid point $G(i, j)$, and $f_{1,1}^{(1+|i-I|),(1+|j-J|)}$ is the response factor for grid $G(1+|i-I|, 1+|j-J|)$ when the detector is above grid point $G(1,1)$. So if the values of the first column of the response factor matrix were obtained, then all the other elements of the response factor matrix could be obtained based on calculation.

The authors define that $\Omega_{1,1}^{i,j}$ is the full detection solid angle for the detector when it measures the radioactivity at grid point, $G(i, j)$, while above grid point $G(1,1)$. This yields

$$f_{1,1}^{i,j} = \frac{\Omega_{1,1}^{i,j}}{4\pi}\eta, \tag{10}$$

where η is the intrinsic efficiency of the detector. The distance between grid $G(1,1)$ and grid $G(i, j)$ was found to be $r=\sqrt{(i-1)^2+(j-1)^2}L$. If one takes the effective radius of the detector as a, based on eqn (2), one gets

$$f_{1,1}^{i,j} = \frac{1}{2}\left(1 - \frac{\sqrt{(i-1)^2L^2+(j-1)^2L^2+h^2}}{\sqrt{(i-1)^2L^2+(j-1)^2L^2+h^2+a^2}}\right)\eta \tag{11}$$

According to eqn (11), one can derive the response factors of all other grid points when the detector is just above grid point $G(1,1)$. Furthermore, one can also get the elements of the response factor matrix according to eqn (9). Below are the results for an unmanned vehicle-mounted monitoring system with the following properties: the intrinsic efficiency of the detector is 100%, the effective detector radius is 5 cm, the detector is 20 m above ground, the grid width is 1 m, and the number of grids in each track is 100. The response factors are shown as Fig. 4.

Since the response factor matrix F was obtained, in the case of real emergency monitoring, if the count rate vector $\dot{N}$ can be obtained, matrix eqn (8) can be solved in order to obtain the activity vector, A. From the activity vector A, the radioactivity distribution on the ground can be known. In a real monitoring situation, the dimension of matrix F is very large. Also, it is noteworthy to point out that the response factor matrix F is always ill-conditioned, since the condition number of matrix F is quite large (the condition number is around 10^{13} when L = 1 m, h = 50 m). Therefore, how to solve this restrictive system quickly and accurately is a key problem (Xue et al. 2000; Salahi 2008). In this referenced work, the equation solver GMRES in Matlab (The MathWorks 2013) is used in order to solve the matrix equation.

SIMULATION FOR ALGORITHM VERIFICATION

Simulation for measurement

Due to the lack of a real monitoring system to experimentally test the algorithm, a computer simulation was used in this work. The basic idea is simulating the detection process in order to get measurement data. Then using the reconstruction algorithm discussed, the activity on the ground can

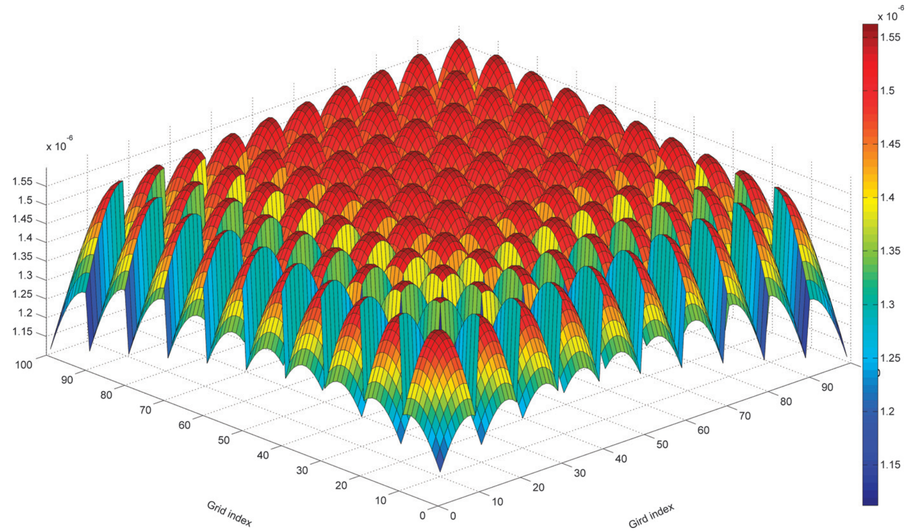

Fig. 4. Response factors.

be reconstructed. Though the computer simulation is not real monitoring, it is reliable enough to verify the algorithms discussed previously. According to previously conducted research, measurement data can be simulated using convolution theory (Lu et al. 2002). For a point source, the count rate at distance r is

$$\dot{N}=\frac{A\Gamma}{r^2}, \tag{12}$$

where Γ is the constant and is equal to the total efficiency for the detector, which is 1 m from a point source. For the surface activity distribution $A(x, y, 0)$, one can build the following infinitesimal model as shown in Fig. 5. The count rate at point (x_1, y_1, h) by this infinitesimal gamma source is

$$d\dot{N}(x_1,y_1,h)=\frac{\Gamma A(x,y,0)dxdy}{(x-x_1)^2+(y-y_1)^2+(0-h)^2}. \tag{13}$$

So

$$\dot{N}(x_1,y_1,h)=\int_{-\infty}^{+\infty}dy\int_{-\infty}^{+\infty}\frac{\Gamma A(x,y,0)}{(x-x_1)^2+(y-y_1)^2+h^2}dx. \tag{14}$$

Note that $H(x_1,y_1,h)=\frac{\Gamma}{x_1^2+y_1^2+h^2}$ is the system response function for the monitoring system. Mathematically, one can write the exposure rate at (x_1, y_1, h) as a two-dimensional convolution. It is

$$\dot{N}(x_1,y_1,h)=A(x_1,y_1,0)\times H(x_1,y_1,h). \tag{15}$$

In real measurement, the measurement noise should be considered. In this work, this issue was addressed by adding a noise term, so eqn (15) could be adjusted as

$$\dot{N}(x_1,y_1,h)=A(x_1,y_1,0)\times H(x_1,y_1,h)+\varepsilon, \tag{16}$$

where ε is the measurement noise. The white noise was considered in this work, and it is created easily by Matlab.

So the following equation set is obtained:

$$\begin{cases}\dot{N}(x,y,h)=A(x,y,0)\times H(x,y,h)+\varepsilon\\ H(x,y,h)=\dfrac{\Gamma}{x^2+y^2+h^2}\end{cases}. \tag{17}$$

In this work, the authors mathematically produce an activity distribution function $A(x, y, 0)$ and detection system response function $H(x, y, h)$. Using these calculations for the convolution using eqn (15) to get the simulated count rate distribution, $\dot{N}(x, y, h)$ can be completed.

A different distribution function, $A(x, y, 0)$, can be produced according to the requirements of the simulation; for instance, the circular uniform surface distributions were produced mathematically in this work to simulate the surface radioactive contamination on the ground.

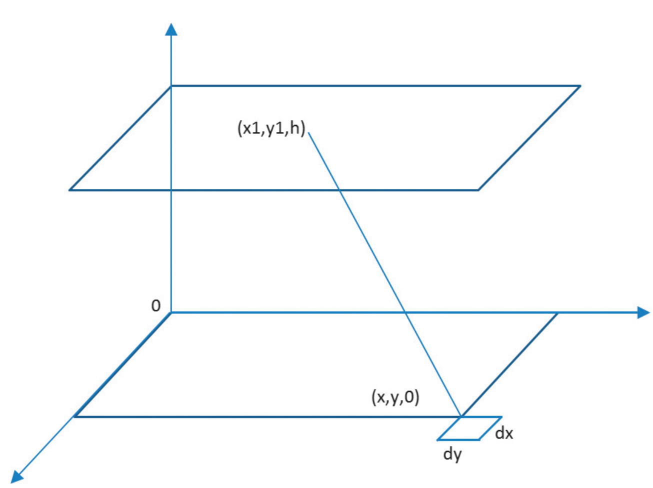

Fig. 5. The exposure model geometry.

Simulation results and discussion

Fig. 6 displays the simulation results when the algorithm was used for reconstructing the single ground contaminated area. The simulation parameters are as follows: effective detector radius 5 cm, grid width 1 m, detection height 20 m, and detection area 100 × 100 m^2. In this simulation, one can assume that there is a circular ^{137}Cs contaminated area with a radius of 10 m on the ground as shown in Fig. 6a. Knowing this convulsion theory can be used to produce the simulated measurement distribution in air when the detection height is 20 m as displayed in Fig. 6c. This effectively shows that it is difficult to tell how the ground contamination is distributed precisely no matter the contamination magnitude and scope. However, Fig. 6d shows that the algorithm performs well in determining the contamination magnitude and scope on the ground. Also, the algorithm can tell the exact location of the contaminated area on ground. As for the magnitude difference between the proposed activity (displayed in Fig. 6a) and reconstructed activity (displayed in Fig. 6d), the difference is

$$\frac{\left|10^5 - 0.96 \times 10^5\right|}{10^5} \times 100\% = 4\%.$$

Fig. 7 displays the simulation results when the algorithm was used for reconstructing the single ground contaminated area. The simulation parameters are the same as the simulation parameters shown in Fig. 6 except for the fact that the detection height is 50 m. In this simulation, one can assume that there is a circular ^{137}Cs contaminated area with a radius of 5 m on the ground as shown in Fig. 7a. Fig. 7c shows that the measurement data will be distributed much more widely than the actual contamination distribution on ground, so it is very hard to tell how the ground contamination is distributed precisely regardless of the contamination magnitude and scope. However, Fig. 7d shows that the algorithm cannot perform well in telling the contamination magnitude, and the reconstructed contamination scope was wider than the actual contamination distribution. One can know that the algorithm can tell the location of the contaminated area on the ground. As for the magnitude difference between the proposed activity (displayed in Fig. 7.a) and reconstructed activity (displayed in Fig. 7d), the difference is

$$\frac{\left|10^5 - 7.5 \times 10^3\right|}{10^5} \times 100\% = 92.5\%.$$

Figs. 8 and 9 show the simulation results when the algorithm was used for reconstructing two ground contaminated areas. The simulation parameters are the same as the simulation parameters shown in Fig. 6. In this simulation,

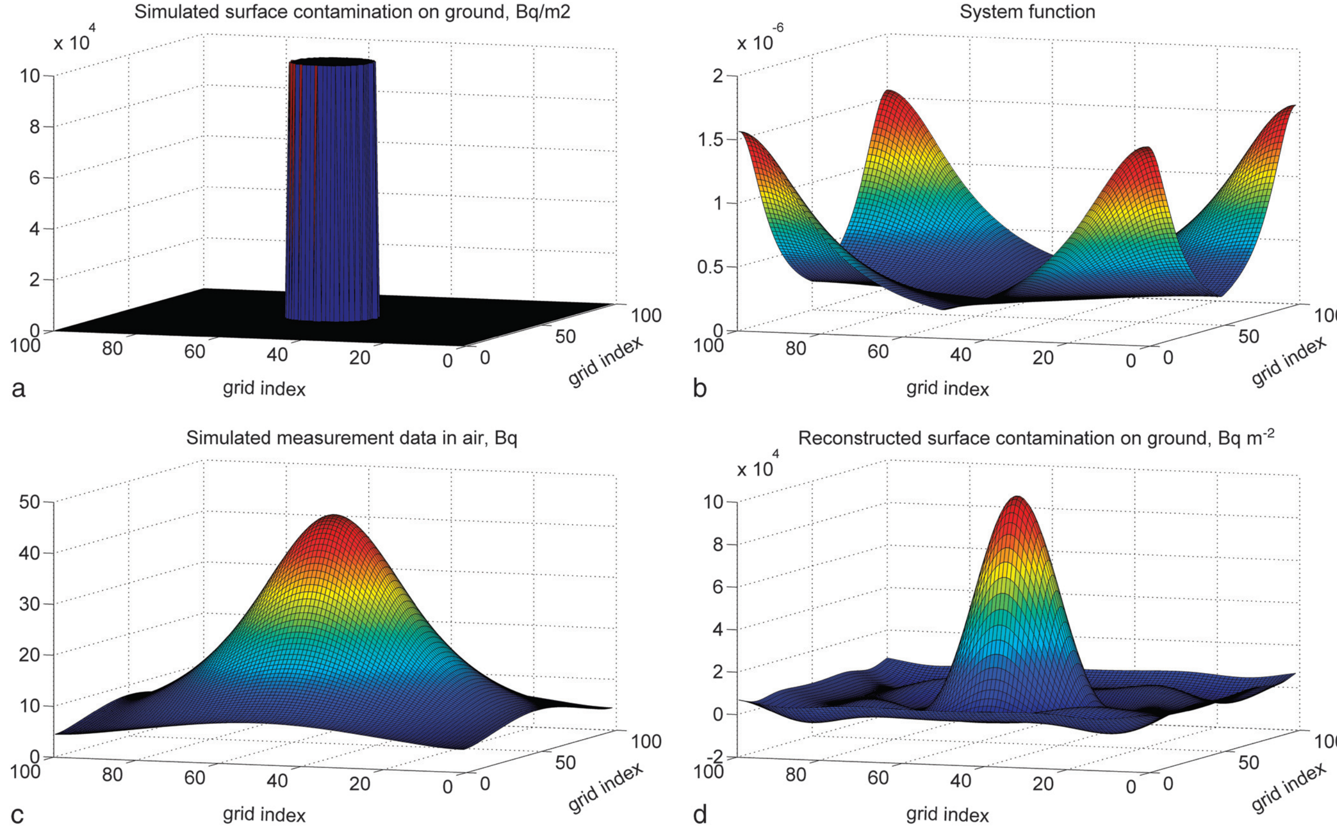

Fig. 6. The simulation results for a single contaminated area (h = 20 m).

one can assume that there are two circular ^{137}Cs contaminated areas with radii of 5 m as shown in Fig. 8a. Fig. 8c shows that the measurement data will be distributed on a much wider scale than that of the actual contamination distribution on the ground. Furthermore, the two contaminated areas were overlapping in the measurement data as shown in Fig. 9c, so it is very hard to tell precisely how the contamination is distributed on the ground regardless of the contamination magnitude and scope. However, as displayed in Figs. 8d and 9d, the algorithm performs well to tell that there were two separate contaminated areas on the ground and the contamination scope and location were reconstructed correctly. Also, the reconstructed contamination magnitude is near the actual contamination magnitude (slightly smaller than the actual). Figs. 8 and 9 show that the algorithm is able to reconstruct the contamination location on the ground correctly when there are two contaminated areas on the ground. As for the magnitude difference between the proposed activity (displayed in Fig. 8a) and reconstructed activity (displayed in Fig. 8d), the difference for these two contamination areas are

$$\frac{|5 \times 10^4 - 1.06 \times 10^4|}{10^4} \times 100\% = 78.8\%$$

$$\frac{|4 \times 10^4 - 8.2 \times 10^3|}{4 \times 10^4} \times 100\% = 79.5\%,$$

Fig. 10 shows the simulation results when the algorithm was used for reconstructing the two ground contaminated areas. The simulation parameters are the same as the simulation shown in Fig. 6. In this simulation, one can assume that there are two circular ^{137}Cs contaminated areas with radii of 5 m as shown in Fig. 10a. Fig. 10c shows that the measurement data will be distributed much more widely than the actual contamination distribution on the ground and that the two contaminated areas overlap in the measurement data as shown in Fig. 10c. With this, it is very hard to tell how the contamination is distributed on the ground precisely, regardless of the contamination magnitude and scope. In this scenario, the algorithm cannot separate the two contaminated area as shown in Fig. 10d; however, the algorithm performs well in that the reconstructed contamination magnitude is around the actual contamination magnitude, which is a little bit smaller than the actual one. As displayed in Fig. 10d, the algorithm can reconstruct where the highest contamination is located, so based on this information, it can tell the contamination location roughly. As for the magnitude difference between the proposed activity (displayed in Fig. 10a) and

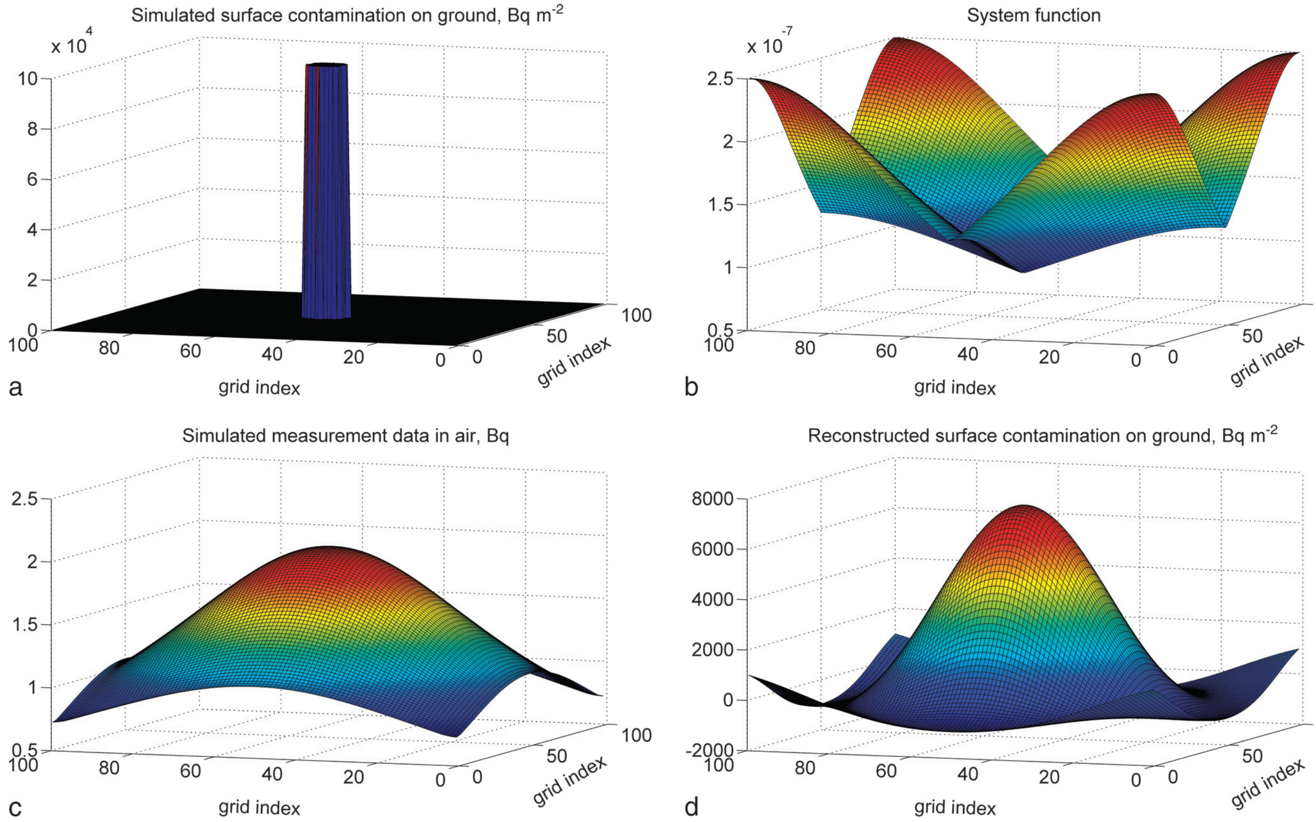

Fig. 7. The simulation results for a single contaminated area (h = 50 m).

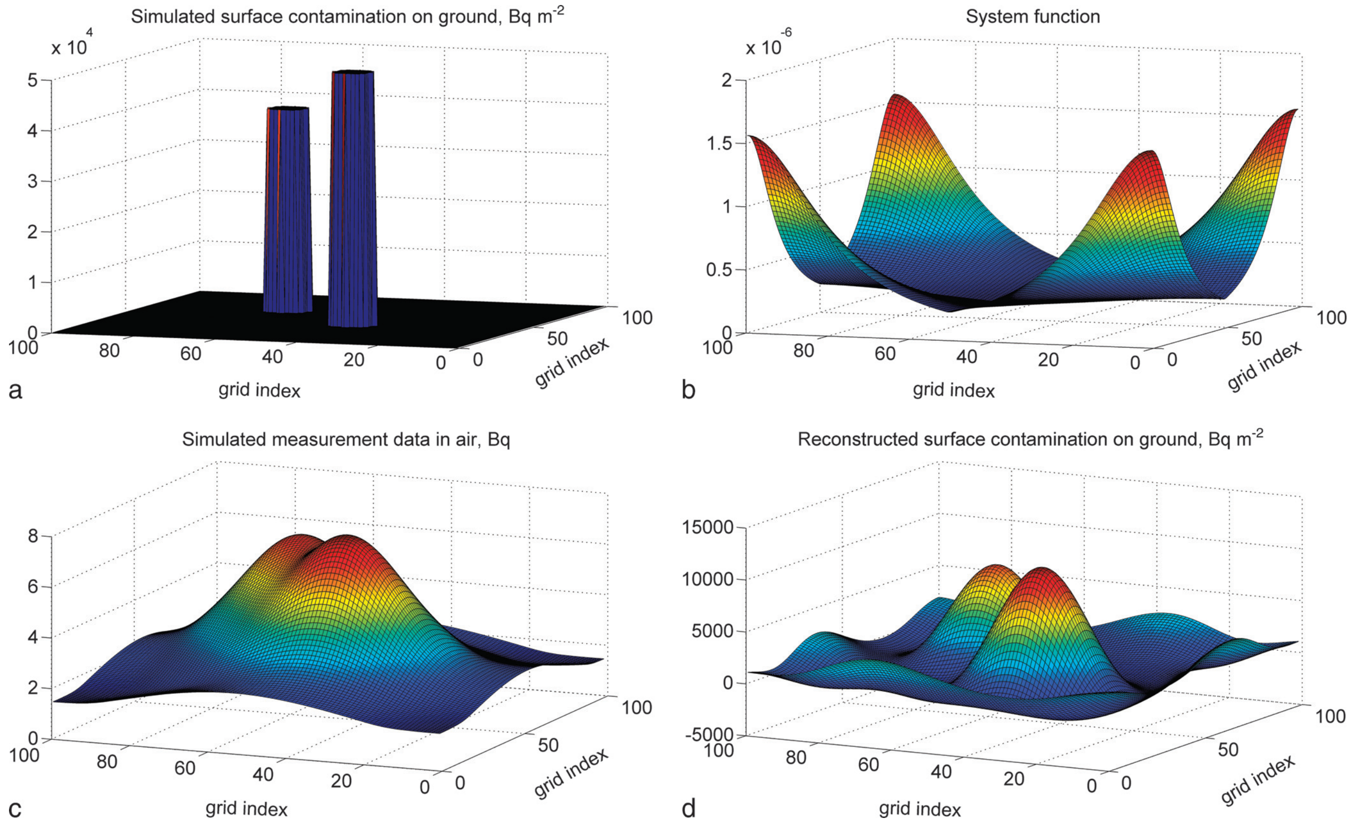

Fig. 8. The simulation results for two contaminated areas (h = 20 m).

reconstructed activity (displayed in Fig. 10d), the difference cannot be simply determined since two contamination areas cannot be separated by algorithm.

It is important to know that the boundary condition is a vanishing boundary; for instance, the proposed contamination distribution was idealized as being circular as displayed

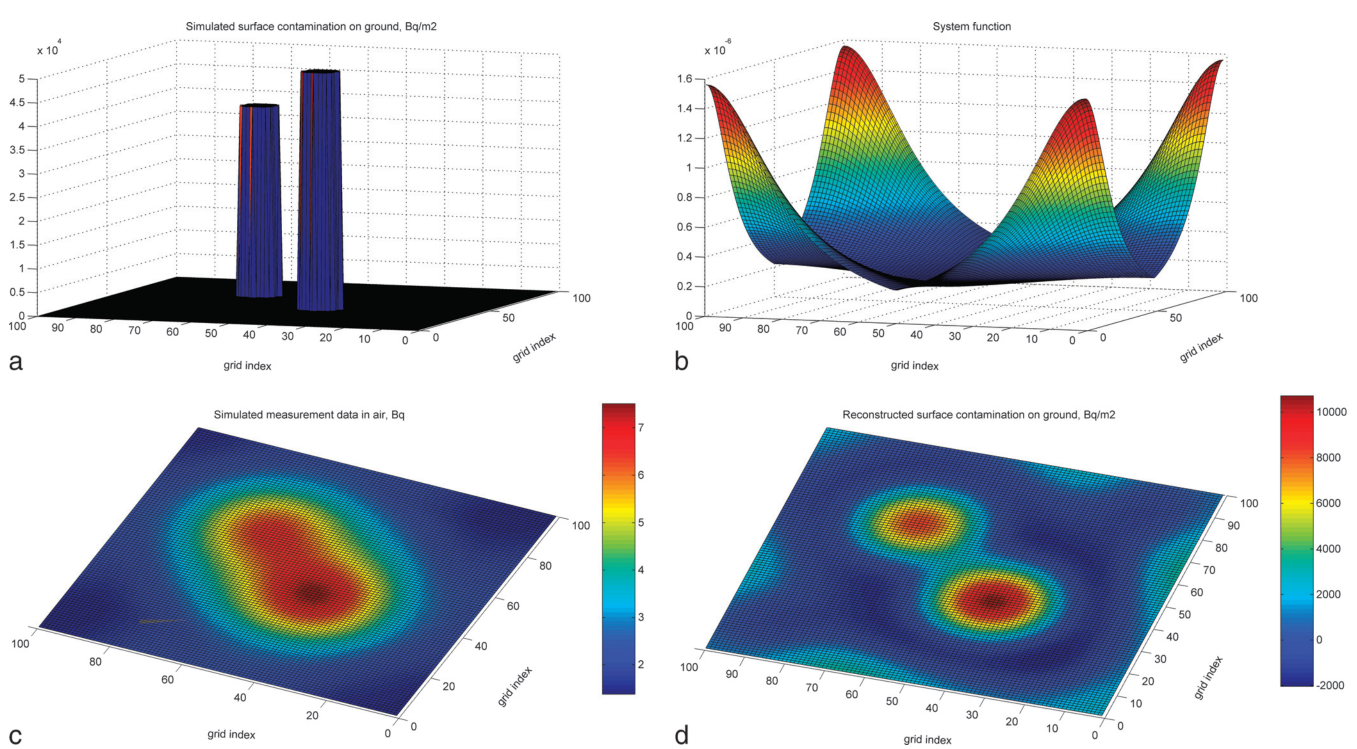

Fig. 9. The simulation results for two contaminated areas (h = 20 m; displayed in plane).

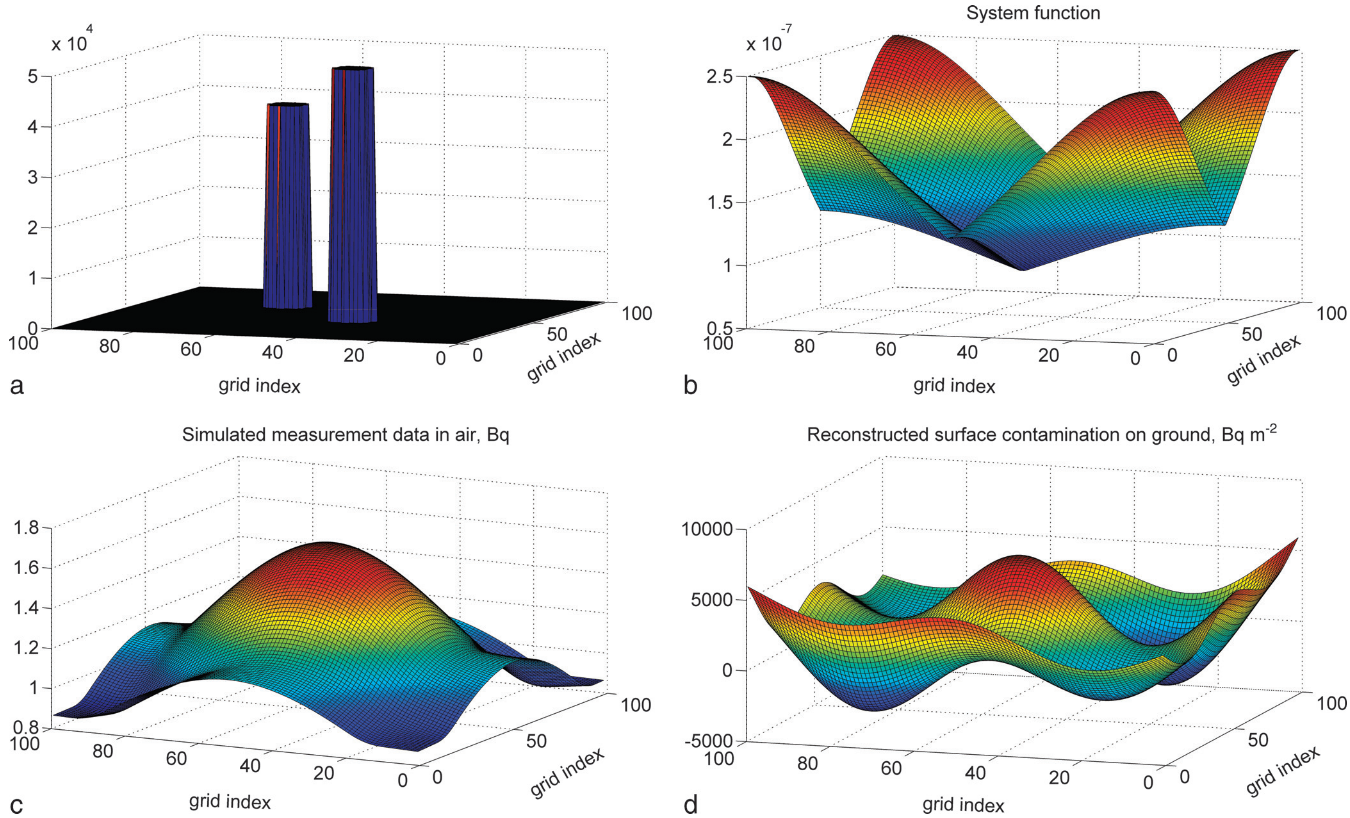

Fig. 10. The simulation results for two contaminated areas (h = 50 m).

in Figs. 6, 7, 8, 9, and 10. It is an idealized condition compared to real measurements, since the real measurements do not vanish and can have substantial magnitude due to environmental radioactivity. A proper way to address the difference between the examples and real measurements could be expanded by measurement data interpolation so as to get a pseudo-idealized vanishing boundary condition. This could be finished by a trivial computation workload, so there is no substantial reason for the application of this method to the real measurements.

CONCLUSION

In this study, one kind of reconstruction algorithm was developed that can be used in nuclear emergency monitoring and decontamination monitoring situations. Due to a lack of in-field testing systems, computer simulations were used to verify the performance of the proposed algorithm. According to the results discussed, it is known that the algorithm performs well in mapping the contamination on the ground based upon the measurement data obtained by the above-ground detection system. The results show that the algorithm also has its disadvantages. For instance, its performance becomes worse when the detection height is over 50 m. However, current emergency detection systems mounted on small, unmanned helicopters usually can fly lower than 50 m. That being said, the algorithm proposed here still qualifies for continued research efforts to be used in in-field radiation monitoring situations.

REFERENCES

Bogatov S, Mazny N. Emergency radiation survey device onboard the UAV. ISPRS. International Archives of the Photogrammetry, Remote Sensing and Spatial Information Sciences XL-1/W2:51–53; 2013. DOI:10.5194/isprsarchives-XL-1-W2-51-2013

International Atomic Energy Agency. The radiological accident in Goiânia. Vienna: IAEA; STI/PUB/815; 1988.

Long S, Martin L, Baylis S, Fry J. Development and performance of the vehicle-mounted radiation monitoring equipment used in the Maralinga rehabilitation project. J Environmental Radioact 76:207–223; 1998. DOI 10.1016/j.jenvrad.2004.03.027.

Lu X, Wang Y, Luo P, Li X, Zhang X. Calculation of radioactive field in nuclear contaminated area from data acquired in aerial survey. Proceedings of the International Conference on Uranium Mining and Hydrogeology III and the International Mine Water Association Symposium, Freiberg, Germany, 15–21 September 2002; New York: Spring Publishing Co.; 2002; 237–246.

Okuyama S, Torii T, Nawa Y, Kinoshita I, Suzuki A, Shibuya M, Miyazaki N. Development of a remote radiation monitoring system using unmanned helicopter. International Congress Series 1276:422–423; 2005. DOI 10.1016/j.ics.2004.11.154.

Pollanen R, Toivonen H, Perajarvi K, Karhunen T, Ilander T, Lehtinen J, Rintala K, Katajainen T, Niemela J, Juusela M. Radiation surveillance using an unmanned aerial vehicle. Applied Radiat Isotopes 67:340344; 2009. DOI 10.1016/j.apradiso.2008.10.008.

Salahi M. On regularization of ill-conditioned linear systems. J Applied Mathematics (Islamic Azad University of Lahijan) 5(17):43–49; 2008.

The MathWorks. Elsevier: MATLAB; 2013.

Sanada Y, Kondo A, Sugita T, Nishizawa Y, Yuuki Y, Iked K, Shoji Y, Torii T. Radiation monitoring using an unmanned helicpter in the evacuation zone around te Fukushima Daiichi nuclear power plant. Exploration Geophysics 45(1):3–7; 2014. DOI: 10.1071/EG13004

Xue XJ, Kozaczek KJ, Kurtzl SK, Kurtz DS. A direct algorithm for solving ill-conditioned linear algebraic systems. Advances X-ray Analysis 42:629–633; 2000.

■■